

γ -Radiation Induced Interstrand Cross-Links in PNA:DNA Heteroduplexes[†]

Tsvetan G. Gantchev,[‡] Sonia Girouard,[‡] David W. Dodd,[§] Filip Wojciechowski,[§] Robert H. E. Hudson,[§] and Darel J. Hunting^{*‡}

[‡]*Department of Nuclear Medicine and Radiobiology, Faculté de Médecine, Université de Sherbrooke, Sherbrooke, Québec, J1H 5N4 Canada, and* [§]*Department of Chemistry, The University of Western Ontario, London, Ontario, N6A 5B7 Canada*

Received February 16, 2009; Revised Manuscript Received May 6, 2009

ABSTRACT: Peptide nucleic acids (PNAs) efficiently hybridize with DNA and are promoted as versatile gene-targeting analytical tools and pharmaceuticals. However, PNAs have never been exploited as radiopharmaceuticals, and radiation-induced physicochemical modifications of PNA:DNA heteroduplexes have not been studied. Drug- and radiation-induced creation of covalent cross-links in DNA obstruct crucial cell survival processes such as transcription and replication and are thus considered genotoxic events with a high impact in anticancer therapies. Here we report that γ -irradiation of complementary PNA:DNA heteroduplexes, wherein the PNA contains L-lysine, free amino, or *N*-methylmorpholinium N- and C-capping groups, results in the formation of irreversible interstrand cross-links (ICL). The number of detected ICL corresponds to the number of available amino functional groups on the PNA. The effect of DNA sequence on the formation of ICL was studied by modifying the terminal nucleotides of the DNA oligonucleotide to create deletions and overhangs. The involvement of abasic sites (ABS) on the DNA strand in the cross-linking reaction was confirmed by independent experiments with synthetic ABS-containing oligonucleotides. Molecular modeling and molecular dynamics (MD) simulations were applied to elucidate the conformation of the N- and C-capping groups of the PNA oligomer and their interactions with the proximal terminus of the DNA. Good agreement between experimental and modeling results was achieved. Modeling indicated that the presence of positively charged capping groups on the PNA increases the conformational flexibility of the PNA:DNA terminal base pairs and often leads to their melting. This disordered orientation of the duplex ends provides conditions for multiple encounters of the short (amino) and bulky (Lys) side chains with nucleobases and the DNA backbone up to the third base pair along the duplex stem. Dangling duplex ends offer favorable conditions for increased accessibility of the radiation-induced free radicals to terminal nucleotides and their damage. It is suggested that the ICL are produced by initial formation of Schiff base adducts between the PNA amino functions and the opposed DNA oxidation-damaged bases or abasic 2'-deoxyribose-derived aldehydic groups. The subsequent reduction by solvated electrons (e^-_{aq}) or other radiation-produced reducing species results in irreversible covalent interstrand cross-links. The simultaneous involvement of oxidizing, $\cdot OH$, and reducing, e^-_{aq} , radicals presents a case in which multiple ionization events along a γ -particle path lead to DNA injuries that also encompass ICL as part of the multiply damaged sites (MDS). The obtained results may find applications in the development of a new generation of gene-targeted radiosensitizers based on PNA vectors.

Inactivation of DNA is the major molecular aim of radiation therapy (RT)¹ as well as most of the common anticancer chemotherapeutics. Double-strand DNA breaks (DSB) formed during RT are assumed to be the crucial lesions for the induction of cell death, although their radiation yield is typically 2 orders of magnitude lower than that of the single-strand breaks (SSB) (1). Intra- and interstrand cross-links (ICL) are another type of DNA damage largely recognized as an action mechanism of a variety of DNA (bis)-alkylating anticancer drugs (nitrogen mustards, nitrosoureas, mitomycin, etc.) (2); however, the potential role of ICL in the RT of tumors has emerged only recently. Thus, it was

shown that radiation and/or specific 2'-deoxyribose oxidation by the radiomimetic antitumoral drug, bleomycin, can produce ICL in vitro and in vivo, as part of the so-called multiply damaged sites (MDS) (3). MDS consist of clustered DNA lesions and include oxidative base modifications, abasic sites (ABS), and the

[†]This research was supported by the Cancer Research Society (Montréal, QC) (D.J.H. and T.G.G.) and the National Sciences and Engineering Research Council (NSERC, Ottawa, ON) (R.H.E.H.).

^{*}To whom correspondence should be addressed. Telephone: (819) 820-6868, ext. 14604. Fax: (819) 564-5442. E-mail: darel.hunting@usherbrooke.ca.

¹Abbreviations: ABS, abasic (AP, apurinic/apyrimidinic) DNA site; ADR, abasic dR; DEG, diethylene glycol (dimer of 8-amino-3,6-dioxaoctanoic acid); CO, complementary oligonucleotide; ICL, interstrand cross-link; MeMor, *N*-methylmorpholinium; MCO, modified complementary oligonucleotide; MDS, multiply damaged sites; MD, molecular dynamics; e^-_{aq} , solvated electron; SSB and DSB, single- and double-strand DNA breaks, respectively; RT, radiation therapy; PNA, peptide nucleic acid; PNA:DNA, heteroduplex composed of one strand of PNA and one strand of DNA; PNA–DNA, heteroduplex covalently linked by an ICL; BrdU, bromodeoxyuridine; MOPAC, Molecular Orbital Package, version 6.0 (QCPE #455 program); VdW, van der Waals; rmsd, root-mean-square deviation; AMN, *N*-amino PNA blocking group; HBN and HEN, 5'- and 3'-DNA termini, respectively; dsDNA, double-stranded DNA; ssDNA, single-stranded DNA.

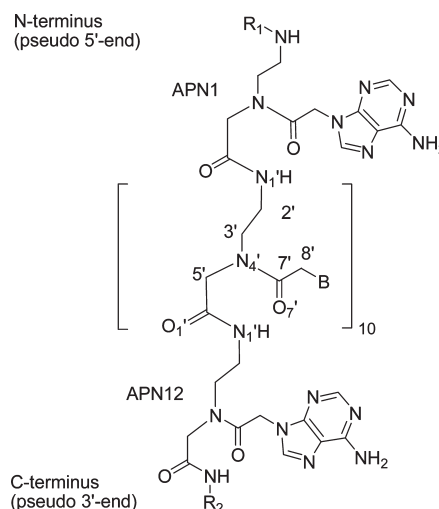
covalent links (cross-links) formed between these entities, together with single- and double-strand DNA breaks. Aldehyde functional groups derived from 2'-deoxyribose ring opening at damaged (abasic) sites are essential in the cross-linking reactions. We have reported the formation of MDS in γ - and UV-irradiated BrdU-substituted dsDNA, including high-yield ICL, when mismatched (bulged) DNA strands were present (4–7). In this particular case, the DNA damage is initiated by interactions of BrdU with solvated electrons (e^-_{aq}) but propagates along the two DNA strands following charge transfer reactions (8). The development of new radiosensitizing techniques aims at amplification of MDS production, including non-DSB (e.g., ICL) to achieve irreparable, specific, and lethal DNA damage in tumor cells.

PNAs are nucleic acid analogues with an uncharged achiral peptide-like backbone consisting of 2-aminoethylglycine-linked monomers, which replace the normal phosphodiester backbone of DNA (9–11). The PNAs were originally conceived as ligands for the recognition of double-stranded DNA, and their unique physicochemical properties allow them to recognize and hybridize to complementary sequences in specific genes and to interfere with the transcription of that particular gene (12–19). PNAs bind to complementary single-stranded DNA in both parallel and antiparallel orientations, and the introduction of chiral centers (bulky charged amino acids, e.g., lysine) improves binding specificity, solubility, and cell uptake (20–23). PNAs have several advantages over oligodeoxy- and oligoribonucleotides. These include higher chemical and biochemical stability (PNAs are not substrates for proteases, peptidases, or nucleases), greater affinity for targets (lack of electrostatic repulsion between hybridizing strands), and higher levels of sequence-specific binding (10, 24). Successful demonstrations of antigene and antisense properties of PNAs are well-documented (12, 13, 15, 18); however, PNA has never been exploited as radiochemotherapeutic agent, since its ability to undergo radiation-induced cross-linking to DNA was not known.

Formation of ICL between PNA and DNA is theoretically possible given the known ability of lysine and other free amino (NH_2) groups to undergo cross-linking reactions with damaged (abasic) or chemically modified DNA (25–29). The cross-linking reaction proceeds via a reversible Schiff base between a DNA aldehydic group and the adjacent ϵ - NH_2 group of lysine or an N-terminal α - NH_2 group. The formation of stable peptide–DNA covalent complexes requires a reducing agent (e.g., sodium borohydride). ABS can result from radiation and chemical action on DNA. The cyclic hemiacetal is the predominant form of the abasic 2'-deoxyribose in DNA duplex (90% cyclic acetal vs 1% acyclic aldehyde) (30–33). Apart from the aldehydic ABS, often termed “true abasic sites”, a range of radiation-induced nucleobase damage evolves in the presence or absence of O_2 to final products bearing aldehydic functional groups (glycols, hydroxyhydantoin and oxoimidazolidines, 5-formyl-2'-deoxyuridine, etc.), in addition to the numerous 2'-deoxyribose oxidation products which may or may not be accompanied by immediate DNA backbone cleavage (34–36).

In this study, we report creation of γ -radiation-induced interstrand cross-links (ICL) in complementary and antiparallel L-Lys-, NH_2 -, and MeMor-modified PNA:DNA heteroduplexes. ICL appear exclusively when the PNA contains the designated capping groups, and their yield is greatly affected by the sequence and conformation of the 3'- and 5'-ends of the DNA. Insights

Scheme 1



into the structure-related determinants, which facilitate or hamper the formation of cross-linked PNA–DNA adducts, were obtained by molecular modeling and molecular dynamics simulations, including DNA possessing abasic sites.

MATERIALS AND METHODS

Peptide Nucleic Acids. PNAs were prepared bearing various charged and/or neutral end groups. The N-terminus was varied among a free amino group (AMN), a lysinyl amine, an acetyl group (Ac), and 4-carboxymethyl-4-methylmorpholin-4-ium (MeMor). The C-terminus was varied among an amide, a lysinyl amide, and the amide of a dimer of 8-amino-3,6-dioxaoctanoic acid (DEG). Scheme 1 presents the general structure of the 12-mer PNA backbone with the sites of modifications (R_1 and R_2) at the N-terminus or head (APN1) and C-terminus or tail (APN12). The experiments were conducted with seven 12-mer PNAs of identical sequence which differed by their capping groups (for structures and sequences, see Table 1). A 15-mer PNA₁₅ of a completely different sequence, PNA-4, served as an independent ICL-negative control in the radiation experiments. All PNA oligomers were synthesized by standard Fmoc-based oligomerization protocols and characterized as previously described (37, 38). The capping lysine residues were always L-isomers.

Oligonucleotides. The oligonucleotides of certified purity were purchased from Invitrogen Inc. and were labeled at the 5'-end with [γ - ^{32}P]ATP using T4 polynucleotide kinase (New England Biolabs) or labeled at the 3'-end with [α - ^{32}P]ddATP using terminal deoxynucleotidyl transferase (TdT, Roche). For the full list of oligonucleotide sequences and abbreviations, see Table 2. Apart from the standard and fully complementary oligonucleotide, CO₁₂, PNA hybridization with the following modified complementary oligomers (MCO) was performed: (i) shorter 11-mer oligomers missing one of the terminal dT, (–5'dT)CO₁₁ and (–3'dT)CO₁₁ (PNA₁₂ strand overhangs), and (ii) a series of longer, 13–16-mer semicomplementary oligomers with extra dA or one or two dT on either the 3'- or 5'-end, or both [DNA strand overhangs (Table 2)]. In addition, two 12-mer oligonucleotides with dR abasic sites located at the first AB1 CO₁₂ or second AB2CO₁₂ position were prepared according to the procedure of Shishkina and Johnson (39). The synthesis of the 3-deoxyhexitol-containing oligos was performed at the University Core DNA Services (University of Calgary, Calgary, AB).

Table 1: PNA Sequences and Structures of C- and N-Terminal Blocking Groups

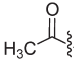
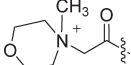
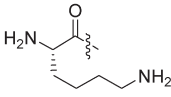
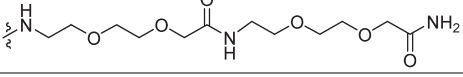
Identity of C- and N-terminal blocking groups		
Ac	Acetyl	
MeMor	N-methylmorpholinium	
K	Lysine	
DEG	dimer of 8-amino-3,6-dioxaoctanoic acid	
Identity of PNA sequences		
PNA Length	Abbreviation	Sequence (N → C)*
12 (or PNA ₁₂)	PNA-1	H ₂ N-K ⁰ -A ¹ T ² G ³ -C ⁴ C ⁵ G ⁶ -A ⁷ T ⁸ C ⁹ -G ¹⁰ T ¹¹ A ¹² -K ¹³ -NH ₂
12	PNA-2A	H ₂ N-K-ATG-CCG-ATC-GTA-NH ₂
12	PNA-2B	Ac-K-ATG-CCG-ATC-GTA-NH ₂
12	PNA-2C	MeMor-K-ATG-CCG-ATC-GTA-NH ₂
12	PNA-3A	H ₂ N-ATG-CCG-ATC-GTA-K-NH ₂
12	PNA-3B	Ac-ATG-CCG-ATC-GTA-K-NH ₂
12	PNA-3C	MeMor-ATG-CCG-ATC-GTA-K-NH ₂
15 (or PNA ₁₅)	PNA-4A	H ₂ N-K-GTT-GGT-ATG-TGC-CGA-DEG-NH ₂
15	PNA-4B	Ac-K-GTT-GGT-ATG-TGC-CGA-DEG-NH ₂
15	PNA-4C	MeMor-GTT-GGT-ATG-TGC-CGA-DEG-NH ₂
15	PNA-4D	H ₂ N-GTT-GGT-ATG-TGC-CGA-DEG-NH ₂
* all oligomers are C-terminal amides. Oligomers are numbered such that the N-terminal PNA residue is number one. Modifications at the N-terminus are referred to as position zero in the text. The numbering system is shown, in superscript, for PNA-1.		

Table 2: DNA and PNA Sequences Used^a

molecules and length	abbreviation	sequence
DNA Sequences Hybridized with PNA ₁₂ (PNA-1, PNA-2, PNA-3), R ₁ -ATG-CCG-ATC-GTA-R ₂		
DNA ₁₂	CO ₁₂	3'-TAC-GGC-TAG-CAX-5'
DNA ₁₁	(-3'dT)CO ₁₁	3'-AC-GGC-TAG-CAT-5'
DNA ₁₁	(-5'dT)CO ₁₁	3'-TAC-GGC-TAG-CA-5'
DNA ₁₃	(+3'dT)CO ₁₃	3'-TTAC-GGC-TAG-CAT-5'
DNA ₁₃	(+5'dT)CO ₁₃	3'-TAC-GGC-TAG-CATT-5'
DNA ₁₃	(+3'dA)CO ₁₃	3'-ATAC-GGC-TAG-CAT-5'
DNA ₁₃	(+5'dA)CO ₁₃	3'-TAC-GGC-TAG-CATA-5'
DNA ₁₄	(+3'dTdT)CO ₁₄	3'-TTTAC-GGC-TAG-CAT-5'
DNA ₁₄	(+5'dTdT)CO ₁₄	3'-TAC-GGC-TAG-CATTT-5'
DNA ₁₆	(+3'/5'dTdT)CO ₁₆	3'-TTTAC-GGC-TAG-CATTT-5'
DNA ₁₂	AB2CO ₁₂	3'-TAC-GGC-TAG-CXT-5'
DNA ₁₂	AB1CO ₁₂	3'-TAC-GGC-TAG-CAX-5'
DNA Sequences Hybridized with PNA ₁₅ (PNA-4A–4D), R ₁ -GTT-GGT-ATG-TGC-CGA-R ₂		
DNA ₁₅	CO ₁₅	3'-CAA-CCA-TAC-ACG-GCT-5'

^a R₁ and R₂ are variable groups as defined in Table 1. X denotes abasic 2'-deoxyribose.

using abasic phosphoroamidite purchased from Glen Research Inc. (Sterling, VA). The final conversion of 3-deoxyhexitol to a dR abasic (ADR) site was performed in our laboratory by oxidation with 5 mM NaIO₄ followed by purification on a G-50 Sephadex microcolumn. The presence of AB sites in 3'-³²P-labeled oligos was verified by hot piperidine treatment and

denaturing polyacrylamide gel electrophoresis (PAGE). In separate experiments aimed at elucidating sequence-dependent effects, PNA-4A–4D bearing different head amino functions were hybridized to their complementary 15-mer oligonucleotide, CO₁₅, and irradiated (Tables 1 and 2). Hybridization of DNA with complementary PNA to form PNA:DNA heteroduplexes and with DNA (DNA:DNA control) in a 1:1 molar ratio was performed by heating the samples to 82 °C for 26 s and cooling them for 54 min. Typically, irradiation was applied immediately after hybridization, unless otherwise stated. The extent of hybridization was routinely verified by nondenaturing (15%) PAGE. A typical example is presented in Figure 1.1 suppl of the Supporting Information.

γ-Irradiation. Aliquots (20 μL, containing 20 pmol of PNA:DNA heteroduplex) in sealed tubes were irradiated using ⁶⁰Co-GammaCell 220 (Atomic Energy of Canada) emitting γ-rays with energies of 1.18 and 1.33 MeV with a dose rate of 2.8 Gy/min. Under standard conditions, samples contained 25 mM EDTA (an •OH radical scavenger) sealed under an atmosphere of N₂ and irradiated. To discriminate between different H₂O radiolysis-derived free radicals involved in the cross-linking process, we performed certain experiments in the presence of O₂ (air), the specific solvated electron (e⁻_{aq}) scavenger, N₂O, and the high-efficiency •OH-radical scavenger, isobutanol (*i*-BuOH).

DNA Damage and ICL Detection. DNA strand breaks and covalent cross-links (ICL) were visualized and quantified using denaturing (sequencing) PAGE. Briefly, following irradiation, samples, mixed with loading buffer, were loaded on a 7 M urea denaturing 20% polyacrylamide gel (35 cm × 43 cm) and electrophoresed for ~2.5 h at 40 W. The phosphorescent screen, exposed to the gel overnight (12 h), was analyzed with a fluorescence scanning system (Storm, Molecular Dynamics, Inc., 100 μm pixel size). For gel quantification, ImageQuant 5.0 (Molecular Dynamics, Inc.) was used.

Molecular Modeling and Molecular Dynamics. Molecular simulations were performed using the Sybyl 8.0 (Tripos Inc.) molecular modeling package. First, the four PNA residues were built, designated as APN, CPN, GPN, and TPN (for the A-, C-, G-, and T-containing units, respectively) and appended to the DNA biopolymer dictionary in Sybyl. The residue coordinates were extracted from PNA:DNA Protein Data Bank entry 1PDT (40) and refined. PNA backbone atoms were assigned MOPAC charges, derived from AM1-Hamiltonian computations, while nucleobase charges were kept as in AMBER7_99. To calculate PNA backbone charges, peptidic fragments were built with N- and C-termini capped with conventional acetyl and N-methyl groups and the side chain capped with NHCOCH₃. Thereafter, the charges of the base–peptide linking atoms (C8', H8'1, and H8'2) were slightly adjusted to make the residues and the backbone separately electroneutral (Figure 2.1 suppl of the Supporting Information). Lysine charges were kept as in the Sybyl (AMBER7_99FF) biopolymer dictionary. The PNA:DNA duplexes of desired sequence containing different charged and neutral N- and C-end groups [amine, lysinyl amine, acetyl, amide, or *N*-methylmorpholinium (Table 1)] were first optimized (Powell gradient) using a distance-dependent dielectric function ($D = 4$). To examine the conformational space occupied by the lysine side chains, we applied the Systematic Torsional Search algorithm in Sybyl, where N-terminal ε- and α-NH₂ groups were range-constrained (3.0–5.0 Å) to the nearest negatively charged atom on the opposing DNA strand (terminal O3' and O2 or O4'

of dT12). Selected molecules were submitted again to energy minimization. Because of the favorable electrostatic interactions of the end groups, such duplexes exhibited the lowest potential energy under vacuum ($E \sim -870$ kcal/mol). Before hydration, an appropriate number of Na⁺ cations were placed 5 Å from the respective phosphorus atom, on the PO₂ angle bisector line to neutralize DNA backbone charges. Due to the electroneutrality of the PNA backbone, no counterions were needed on this strand; however, lysine ε- and α-NH₂ groups were considered positively charged (pH 7). Three additional Na⁺/Cl⁻ pairs were added at random near the 3'- and 5'-DNA termini. Molecules were hydrated using the SilverWare hydration routine of Sybyl. The hydration box size in SilverWare is controlled either by the nonbonded cutoff of the electrostatic interactions or by the number of hydration shells. A NBD cutoff of 12 Å with 25 hydration shells was used. A typical box size was ~54 Å × 80 Å × 66 Å, containing ~9670 TIP3P water molecules of ~1.05 g/cm³ initial density, which changed to ~0.97 g/cm³ after the MD heating phase. Before standard MD, solvated PNA:DNA duplexes were subjected to simulated annealing of 5–10 heating/quenching steps (350–200 K, NTV, canonical ensemble, Figure 2.2 suppl of the Supporting Information), followed by energy minimization. Thereafter, selected molecules were submitted to unconstrained MD (up to 300 ps) using an isobaric (NTP) thermodynamic ensemble as previously described (41). Analysis was performed using Sybyl analytical tools (dynamics tables, spreadsheets, graphics, etc.). Because of the initial simulated annealing and the removal of possible solution-solute strains, the thermodynamic equilibrium during molecular dynamics runs was achieved within ~100 ps (for thermodynamic trajectories, see Figure 4 suppl of the Supporting Information).

RESULTS

Radiation-Induced ICL in PNA:DNA Heteroduplexes: Effect of PNA End Capping Groups. All seven PNA molecules, PNA-1–PNA-3, were hybridized with the complementary oligonucleotide, CO₁₂ (Scheme 1 and Tables 1 and 2), and subjected to 750 Gy γ-radiation. As shown in Figure 1A, a series of slowly migrating bands, representing PNA–DNA interstrand cross-links (ICL), appears when γ-irradiated heteroduplexes were analyzed by denaturing PAGE. Cross-links do not appear following irradiation of single-stranded DNA, PNA, or a DNA:DNA duplex. The appearance of some minor bands (Figure 1A) may result from the presence of impurities in the oligonucleotides. In high-resolution gels, DNA cross-linked with PNA-1 usually presented three separated bands, labeled I, II, and III (top to bottom, Figure 1B). Occasionally, more diffused bands also appear but were difficult to quantify. PNA-2A always gave two well-separated bands (I and II), while PNA-2B and PNA-2C gave smears. DNA cross-links with the PNA-3 series give rise to PNA-3A [two bands (II and III), of which II is of higher intensity], PNA-3B [always one band (III)], and PNA-3C [usually two bands of similar intensity (III and IV)]. Figure 2 presents individual and total band intensity with an account of the overall radioactivity. Because the PNA sequences differ only by their N (pseudo-5') and C (pseudo-3') end-capping groups, it is obvious that both the quantity and intensity of the ICL bands observed in irradiated heteroduplexes depend on the structure and interactions of these capping groups with the opposing and radiation-modified 3'- and 5'-end nucleotides of DNA. Concomitant with the formation of PNA–DNA interstrand

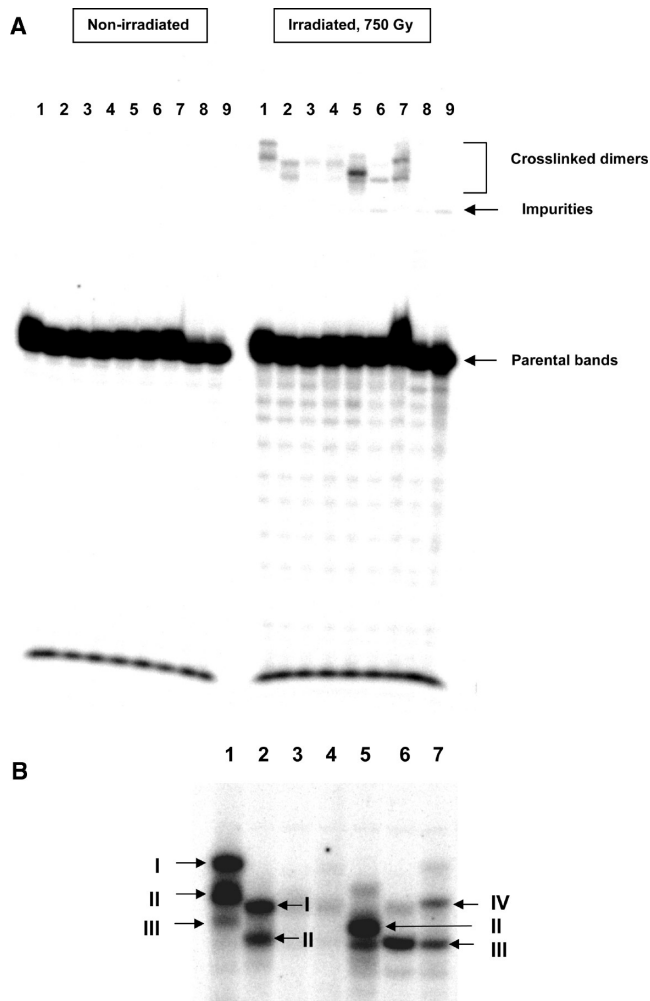


FIGURE 1: (A) Full-scale denaturing PAGE gels: non-irradiated (left) and irradiated (right) samples. (B) Enlarged gel scan presenting the covalent PNA–DNA dimer (ICL) area only. Aqueous solutions of [^{32}P]CO $_{12}$ hybridized with various PNA were γ -irradiated (750 Gy) under a N $_2$ atmosphere in the presence of 25 mM EDTA. Samples in lanes 1–7 differ only by the type of capping groups on PNA ends: (1) PNA-1, (2) PNA-2A, (3) PNA-2B, (4) PNA-2C, (5) PNA-3A, (6) PNA-3B, and (7) PNA-3C. Lane 8 was the dsDNA control (CO $_{12}$ hybridized to a complementary oligonucleotide), and lane 9 contained ssDNA (CO $_{12}$ alone).

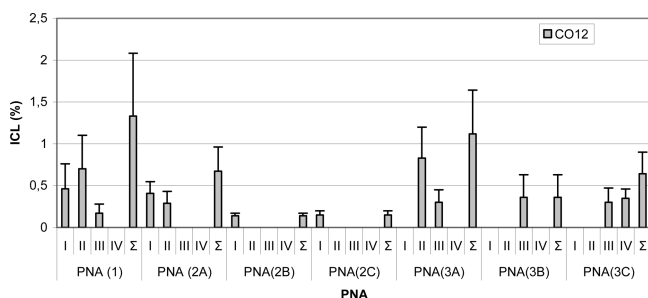


FIGURE 2: Yields of covalent PNA–DNA dimers (intensities of ICL bands I–IV and their sum, Σ) in the seven PNA-1–3:CO $_{12}$ heteroduplexes. Averaged data from four independent experiments.

cross-links, radiation-induced DNA strand breaking results in full-scale degraded oligonucleotide ladders (Figure 1A, bottom). Since only the DNA is radioactive and thus visualized, it is unknown if PNA is also degraded during irradiation. The comparative analysis of the enumerated ICL band mobility with

respect to PNA composition (charge, MW, and overhangs; see below) indicates that the majority of PNA–DNA covalent complexes likely contain full chain polymers. On the other hand, diffuse bands and smears likely originate from assembly of cross-linked adducts of different chain lengths. The analysis of the ICL band pattern from different PNA:DNA heteroduplexes allowed us to assign the origin of the individual bands, at least with respect to the participating end groups on the PNA strand; the possible partner groups on the DNA strand are discussed in the next sections. Band I requires the presence of PNA head Lys(0); band II requires the presence of the PNA N-end α -NH $_2$ group, while band III is associated with the PNA tail, Lys(13). It is noteworthy that band II is generally the most intense. Band IV appears only in PNA-3C:DNA heteroduplexes and obviously arises from radiation-induced interactions and alterations of the *N*-methylmorpholinium (MeMor) PNA headgroup. Interestingly, this band did not appear when Lys(0) and MeMor were simultaneously present, as in PNA-2C (this disparity will be discussed below). It is likely that the ICL band pattern represents migration of covalently linked heteroduplexes, each with a single ICL, originating from the interaction of a designated PNA capping group with closely positioned radiation-modified nucleotides on the DNA strand. The explanation of the various gel mobilities of the different PNA:DNA dimers is based on the following arguments. The gel migration of the covalent DNA–PNA complexes depends on their net charge, MW, and conformational factors, i.e., polymer flexibility, nonlinearity, etc. As expected and confirmed by our molecular modeling studies, the flexibility of duplex heads (PNA N-termini and 3'-DNA ends) is greater than that of the duplex tails (PNA C-termini and 5'-DNA ends). It is therefore suggested that a cross-link formed with the participation of Lys(0) would be more flexible than that formed by Lys(13), and thus under all other equal conditions, the ICL I band would exhibit retarded gel mobility with respect to the ICL III band. On the other hand, the NH $_2$ group provides a shorter linker (less flexibility), and thus, it is reasonable to assume that the ICL II band would migrate faster than the ICL I band. Free lysinyl side chains would slow band migration due extra positive charge, increased flexibility, and/or increased MW. These considerations are consistent with the band assignment presented in Figure 1B. Thus, within the covalent dimers formed between DNA and partners from the PNA A and B series (Table 1), there is a negligible difference in polymer MW and charge, assuming that the N-terminal NH $_2$ groups are nearly deprotonated at pH 8. As seen in Figure 1B, the ICL III dimer migrates faster than the ICL II dimer (lane 6 vs lane 5), while the ICL I band moves slower than the ICL II band (lane 2 vs lane 3), etc. The PNA-1–DNA covalent dimers are less mobile due to the presence of at least one unreacted lysinyl residue. The working hypothesis we tested is that the detected ICL arise from the initial formation of Schiff bases between PNA amino groups and radiation-damaged (aldehydic) nucleotides, or ABS on the DNA strand. The Schiff bases are further transformed to corresponding more stable reduced compounds by radiation-induced reduction, likely via solvated electrons, e^-_{aq} .

Effect of DNA Composition (overhangs and sequence). To further elucidate the origin and radiation efficiency of ICL production with respect to the DNA end nucleotides opposing the NH $_2$, Lys, or MeMor PNA end groups, we performed experiments in which the same series of seven PNAs (PNA-1–PNA-3) which were hybridized with 3'- and 5'-end-modified complementary oligonucleotides [MCO (Table 2)] and then

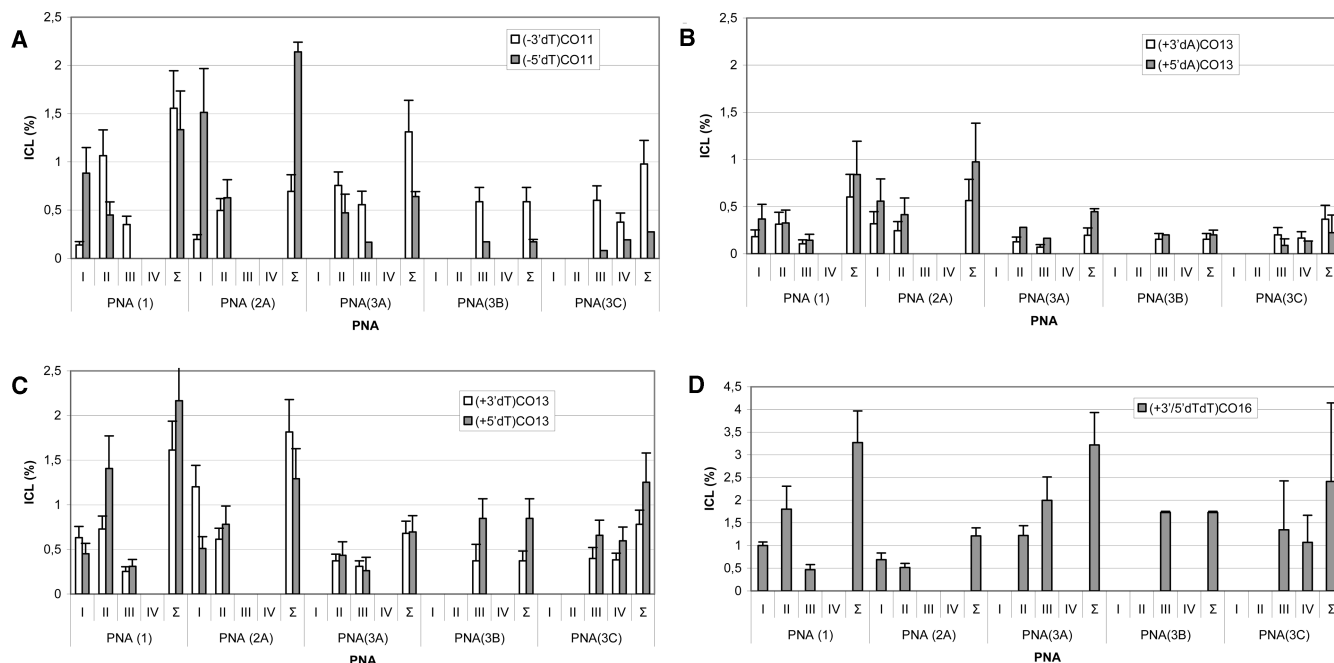


FIGURE 3: Yields of ICL in PNA:MCO complexes. (A) PNA overhangs: PNA:(-3'dT)CO₁₁ and PNA:(-5'dT)CO₁₁. DNA overhangs: (B) PNA:(+3'dA)CO₁₃ and PNA:(+5'dA)CO₁₃, (C) PNA:(+3'dT)CO₁₃ and PNA:(+5'dT)CO₁₃, and (D) PNA:(+3'/5'dTdT)CO₁₆. Data for PNA-2B and -2C have been omitted because of the low intensity (<0.15%). Averaged data from three or four independent experiments. For examples of statistical variance and significance of mean differences (*t* test), see the Supporting Information (Table 1 suppl).

irradiated. The selected MCO form heteroduplexes with unpaired (single-stranded) regions at one or both duplex ends. This experimental design allowed us to compare sequence effects on the cross-linking reaction (e.g., dT vs dA termini), to compare susceptibilities of duplex ends to radiation damage, and to assess the role of the conformation of the end regions.

In the PNA:(-3'dT)CO₁₁ heteroduplex, ICL band I apparently arising from the interaction of the N-Lys(0) with the 3'-end of the DNA is diminished (Figure 3A) as compared to that of the normal PNA:CO₁₂ duplex (Figure 2). Similarly, the ICL III band in the PNA-1:(-5'dT)CO₁₁ heteroduplex almost disappears, and its magnitude is greatly reduced in other duplexes. Apparently, the α -NH₂-dependent band (II) is the least sensitive to these modifications. With PNA:(+5'dA)CO₁₃ and PNA:(+3'dA)CO₁₃ heteroduplexes, containing dA overhangs, an overall decrease in band intensities was observed as compared with the CO₁₂ control; notably, bands I and II in PNA-1 and bands II and III of the PNA-3A–DNA dimer were suppressed by approximately one-half (Figure 3B). However, in heteroduplexes with single or double 3'- or 5'-end dT overhangs, and especially with the PNA:(+5'/3'-dTdT)CO₁₆ duplex possessing double overhangs, a significant increase in ICL yields of the individual bands and in total conversion was obtained (Figure 3 C,D and Figure 1.2 suppl of the Supporting Information). The large standard deviations recorded in some experiments prompted us to compare the actual differences between different (overhang) groups using the two-tail Student's *t* test. The evaluation of the "null hypothesis" at the *P* = 0.05 level proved the statistical significance of the mean differences in the majority of cases reported in Figure 3 (for an example, see Table 1 suppl of the Supporting Information). In summary, the results described above indicate that 5'- and 3'-terminal dT residues and/or their radiation-damaged derivatives play an important role in the generation of the interstrand cross-links.

When the 15-mers PNA-4A–4D (Tables 1 and 2) were hybridized to their DNA₁₅ oligonucleotide and were subjected

to γ -irradiation, no ICL were detected (Figure 1.3A,B suppl of the Supporting Information). This negative control emphasizes the role of PNA N- and C-termini versus 3'- and 5'-end DNA composition in ICL formation.

Effect of Free Radical Scavengers, pH, and Counterions. The free radical species (\cdot OH, \cdot H, and e^-_{aq}) generated during γ -radiolysis of H₂O interact with and damage DNA nucleobases and 2'-deoxyribose to different extents. The most extensive damage is attributed to \cdot OH radicals (34). An insight into the irradiation-induced processes involved in the formation of DNA–PNA cross-links was obtained by observing the effects of different free radical scavengers. During preliminary experiments, we established that anaerobic irradiation conditions in the presence of the moderately efficient \cdot OH radical scavenger EDTA resulted in higher ICL yields. Comparative results from experiments in which PNA:DNA duplexes were irradiated under N₂, N₂O, or O₂ (air) atmospheres, and/or in the presence of EDTA and *i*-BuOH (as \cdot OH radical scavengers), are presented in Figure 4. It is evident that the most favorable environment for generating high-yield ICL involves anaerobic conditions in the presence of \cdot OH radical scavengers. Both \cdot OH scavengers are sufficient to enhance the ICL yields, but the presence of 2% (v/v) *i*-BuOH [$k(\cdot$ OH + *i*-BuOH) = 3.3×10^9 L mol⁻¹ s⁻¹] during radiation is superior to 25 mM EDTA [$k(\cdot$ OH + EDTA) = 4×10^8 L mol⁻¹ s⁻¹] (42). Importantly, N₂O conversion of e^-_{aq} to \cdot OH following the reaction $e^-_{aq} + N_2O + H_2O \rightarrow OH^- + N_2 + \cdot$ OH ($k = 9.1 \times 10^9$ L mol⁻¹ s⁻¹) suppresses ICL formation. It is therefore evident that e^-_{aq} , a strong reducing radical [$E^\circ_{red} = -2.9$ V (43)], or possibly secondary base anions play an essential role in the PNA:DNA cross-linking reaction.

We also found that slightly alkaline solutions (pH 8) and a lower counterion concentration, e.g., 10 mM versus 20–100 mM phosphate buffer, enhance the ICL yield. This is in accord with the findings showing the importance of e^-_{aq} in the cross-linking reaction; the e^-_{aq} lifetime is increased under alkaline solutions, as

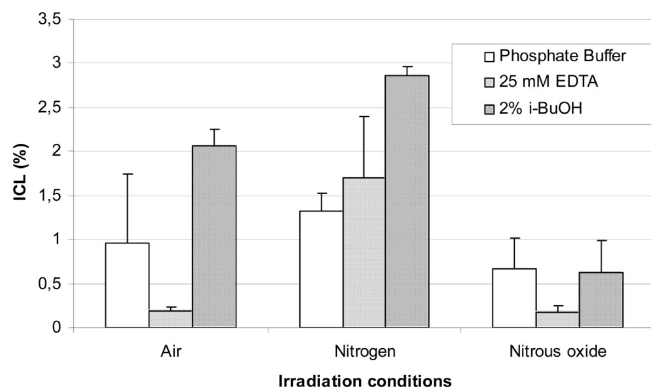


FIGURE 4: Effect of free radical scavengers, EDTA, *i*-BuOH, and N_2O , and the presence of O_2 on the total radiation-induced ICL yield (bands II and III) in the PNA-3A:CO₁₂ duplex. Averaged data from three experiments: (white bars) phosphate buffer only, (light gray bars) phosphate buffer with 25 mM EDTA, and (dark gray bars) phosphate buffer with 2% (v/v) *i*-BuOH.

is the lifetime of nucleobase anion radicals, generated after reduction by e^-_{aq} (34, 44). Since the reaction between aldehydes and amines to form a Schiff base and its subsequent reduction require a slightly acidic environment (45), it follows that in the situation presented here, the more critical factor to achieve high-yield irreversible cross-links is the abundance of reducing species.

ICL Formation in ABS-Containing Heteroduplexes. Hydrolysis of the N-glycosidic bond of a damaged nucleobase yields an abasic site (ABS), the most common DNA lesion under γ -radiation (34). To examine the possible role of ABS as partners in the cross-linking reaction with PNA amino-capping groups, we performed experiments with synthetic abasic oligonucleotides (ABCO₁₂). These ABCOs were constructed by replacement of one of the two nucleotides, dA2 or dA1, to yield AB2CO₁₂ or AB1CO₁₂, respectively (Table 2). The experiments were performed without radiation; instead, a chemical reduction of the presumed Schiff base with borohydride was used to form stable, reduced compounds as final products. With the aim of increasing the ICL yields, we performed experiments using different conditions, e.g., temperature and incubation time, as well as an interchange of the reducing agent (NaBH₄ vs NaCNBH₃; for details, see the legend of Figure 5). The gel analysis (Figure 5A,B) indicates that hybridization of AB2CO₁₂ with PNA-1 containing C-end Lys(13) produces ICL, while PNA-2B which lacks Lys(13) reacts poorly. In contrast, hybridization of AB1CO₁₂ with PNA-1 and PNA-3B results in ICL, while PNA-2B does not. This confirms that damaged sites in DNA, in this case synthetic ABS, are involved in the formation of a Schiff base with the amino groups of the corresponding capping PNA residues. Figure 5C shows an enlarged ICL migration zone of a gel where selected PNA:CO₁₂ samples subjected to γ -radiation comigrated with the corresponding PNA:AB2CO₁₂ heteroduplexes treated with NaCNBH₃. There is a good conformity between the migration patterns of the radiation-induced and chemically induced ICL bands. The experiments with ABCOs confirm the correctness of the ICL band assignment, as related to the participation of the individual PNA amino-capping groups (Figure 1B). In addition, the results point out that AP sites on DNA, formed by base loss, are likely involved in ICL generation under radiation. Formation of ICL was also detected when DNA, preirradiated under different conditions, was hybridized to various PNAs, followed by reduction with borohydride.

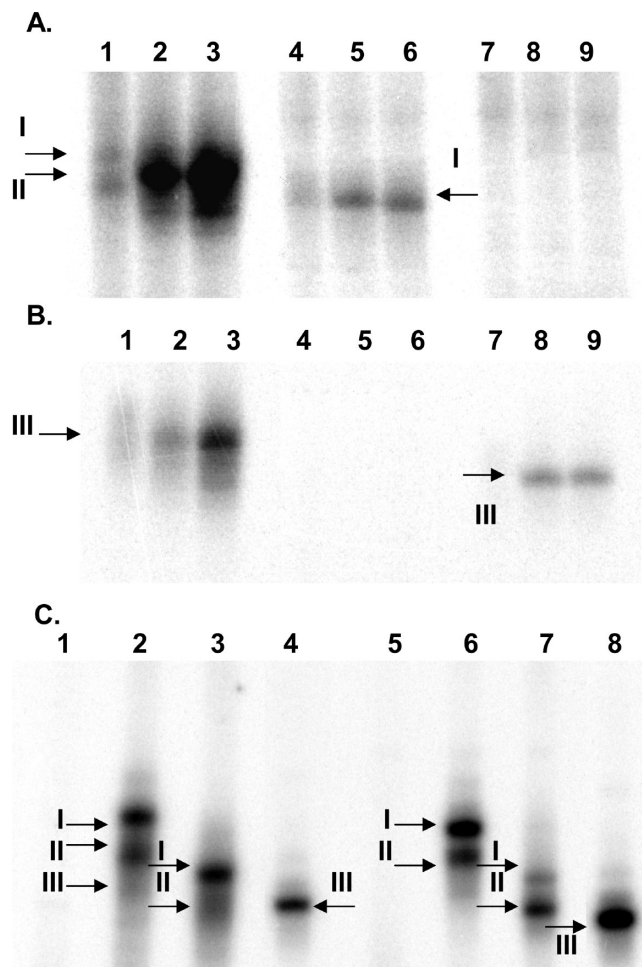


FIGURE 5: Zoomed denaturing PAGE gel scans showing ICL bands obtained from PNA-1, -2B, and -3B hybrids with ABS-containing oligonucleotides: (A) AB2CO₁₂ and (B) AB1CO₁₂ and treatment (or not) with NaBH₄ (100 mM for 5 min at room temperature, or at an elevated temperature, 37 °C). PNA-1, lanes 1–3; PNA-2B, lanes 4–6; PNA-3B, lanes 7–9. Samples in lanes 1, 4, and 7 were not treated with NaBH₄; in lanes 2, 5, and 8, samples were treated with NaBH₄ at ambient temperature, and in lanes 3, 6, and 9, samples were treated with NaBH₄ at 37 °C. In the PNA-1:AB2CO₁₂ duplex, two closely migrating ICL bands (I and II) were formed, indicating that Lys(13) and α -NH₂ likely interact independently with the abasic deoxyribose, dR2; the PNA-2B:AB2CO₁₂ duplex gives one band (I), and PNA-1 and PNA-3B when hybridized with AB1CO₁₂ give also one band (C) Comigration of PNA–CO₁₂ covalent dimers produced by γ -radiation (lanes 1–4) and the related PNA–ABCO₁₂ dimers (lanes 5–8) generated after chemical reduction with 50 mM NaCNBH₃ (2 h at 37 °C): PNA-1:CO₁₂ (lane 2), PNA-2A:CO₁₂ (lane 3), PNA-3B:CO₁₂ (lane 4), and the corresponding PNA:ABCO₁₂ duplexes, PNA-1:AB2CO₁₂ (lane 6), PNA-2A:AB2CO₁₂ (lane 7), and PNA-3B:AB2CO₁₂ (lane 8). Lanes 1 and 5 contained γ -irradiated ssCO₁₂ and NaCNBH₃-treated ssAB2CO₁₂, respectively. A comparison with the results from panels A and B indicates that treatment with NaCNBH₃ tends to produce higher yields and better ICL band resolution.

However, incomplete hybridization in these samples hampered quantitative analysis (data not shown).

Structure of PNA:DNA Duplexes from Molecular Modeling and MD Simulations. In line with our experimental findings, the most intriguing part of the structure modeling was the elucidation of the dynamic behavior of the PNA capping groups and their interactions with opposing end nucleotides on the DNA strand. The initial (vacuum-minimized) structure of the PNA-1:DNA(CO₁₂) duplex is shown in Figure 6A (for the

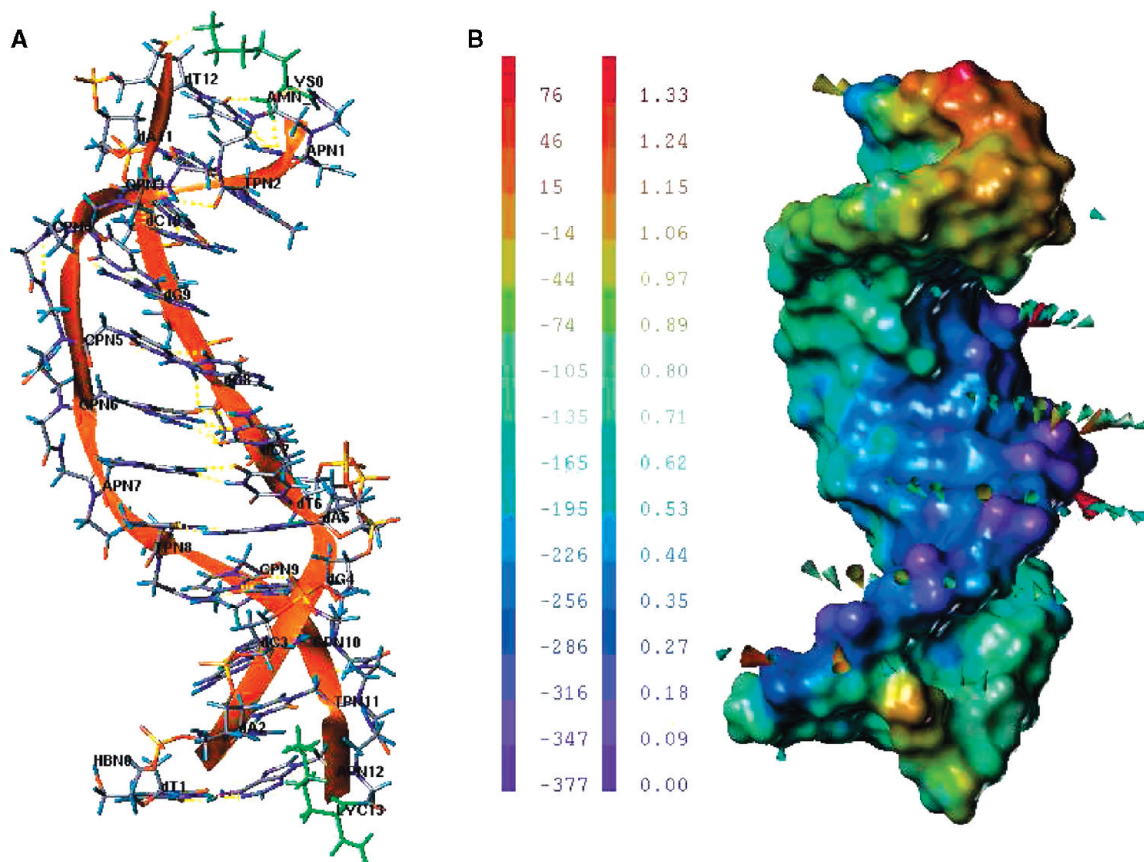


FIGURE 6: (A) Starting three-dimensional structure of the right-handed PNA-1:DNA(CO₁₂) heteroduplex. PNA and DNA are in an antiparallel orientation. The duplex head (top) contains two N-terminally charged groups, ϵ -NH₃⁺ of Lys(0) and α -NH₃⁺ (AMN-1) (both colored green); at the duplex tail (bottom), the PNA C-end is capped by the single charged Lys(13) and amide (both colored green) (see also Scheme 1). DNA ends are uncharged. Atoms are in atom-type color; the backbone ribbon is colored orange. The Lys(0) side chain bridges the two strands, and this configuration is enforced by the electrostatic interaction of the ϵ -NH₃⁺ group with DNA O3'H end group. The α -NH₃⁺ group (AMN-1) orientation is stabilized by H-bonding interactions with the terminal APN1 and dT12 monomers. The Lys(13) side chain is in the minor groove, and the ϵ -NH₃⁺ group is in electrostatic interactions with the negatively charged atoms of the dA2 residue; this Lys(13) orientation is also constrained by a H-bond between the C-amido group and the N1' atom of the APN12 backbone. (B) PNA:DNA duplex electrostatic potential (Connolly surface) and electric field (cones). Note the high electronegative potential on the DNA backbone and the positive charge at the duplex ends. Electrostatic potential ramps: kilocalories per mole per electron, outer scale; electric field, volts per angstrom, inner scale. The surface was built using Sybyl-MOLCAD.

conformational details, see the legend). It was also interesting to map the steric–electrostatic properties of the PNA:DNA heteroduplex. Figure 6B shows the color-coded electrostatic Connolly surface and the electrostatic field generated by the unevenly charged duplex: DNA-electronegative and PNA-neutral, but with positively charged edges (protonated ϵ - and α -NH₃⁺ groups). Although in solution and in the presence of counterions this high degree of polarization is reduced, at close distances negatively charged radiation-produced species, such as e^-_{aq} , would be strongly attracted to the PNA:DNA edges and repulsed by the highly negative DNA backbone.

The Lys(0) orientation, as presented in Figure 6A, was metastable due to the high torsional and unfavorable VdW interaction energies, although compensated by the electrostatic energy contribution. In contrast, the Lys(13) conformation was both sterically and electrostatically more favorable, additionally stabilized by backbone H-bonding (HN1'–O7' and HN1'–O1'). Pronounced dynamic flexibility, especially of the N-PNA end, encompassing not only Lys(0) but also the terminal PNA:DNA base pairs, was revealed by the MD simulations. The dynamic distance trajectories and PNA:DNA structures, averaged over the last 50 ps (of 200 ps MD runs), show that there is a rapid reorientation of Lys(0) from the starting position shown in

Figure 6A, down along the minor groove formed by the three terminal nucleotide pairs (Figure 7A). The distance between the ϵ -NH₃⁺ nitrogen atom (NZ) of Lys(0) and the C2 atom of dC10, the third DNA nucleotide from the 3'-end, may be as short as ~ 3.5 Å (Figure 8A). At the same time, the α -NH₃⁺ group (AMN-1) forms various short-distance contacts with the bases of the second (from head) base pair, TPN2:dA11 (Figures 7A and 8A). The side chain of the PNA C-end lysinyl residue, Lys(13), fluctuates close to the 5'-dT1 and dA2 nucleotides and more often is positioned along the minor groove than is exposed to the solvent (Figures 7B and 8B).

The dynamic structure of a PNA:DNA heteroduplex with two simultaneous AB sites at the second and eleventh DNA positions [(AB2AB11)CO₁₂] was also modeled and studied. The dynamic reorientation of the two capping lysines was similar to that observed with the PNA-1:CO₁₂ duplex: the ϵ -NH₃⁺ nitrogen (NZ) of Lys(0) rapidly comes into close contact with the O1' atom of ADR11; the AMN-1 group forms a H-bond contact with the T12 base; while despite fluctuations, the NZ atom of Lys(13) remains close to the O1' atom of ADR2 (Figures 7C,D and 8C and Figure 2.8 suppl of the Supporting Information). In contrast to the uncharged, acetyl-terminated PNAs, molecules containing at least one positively charged group at the N-terminus, the two

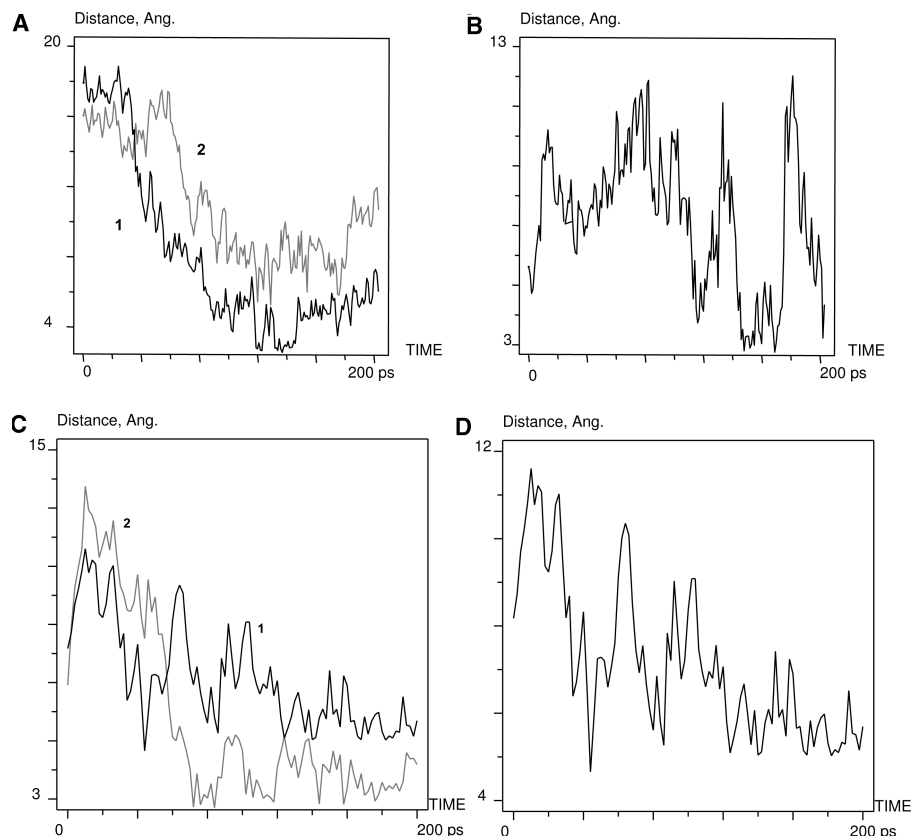


FIGURE 7: Reorientation of head and tail capping groups during 200 ps MD runs and their move toward nucleotides on the DNA strand. Distance trajectories in the PNA-1:CO₁₂ duplex: (A) distance between the α -NH₃⁺ nitrogen and the O2 atom of dC10 (black, 1) and distance between the ϵ -NH₃⁺ nitrogen (NZ) of Lys(0) and the O4' atom of dC10 (gray, 2) and (B) distance between the NZ atom of Lys(13) and the O4' atom of dT1. Distance trajectories in the PNA-1:(AB2AB11)CO₁₂ duplex: (C) distance between the α -NH₃⁺ nitrogen atom and the O1' atom of ADR11 (black, 1) and between the NZ atom of Lys(0) and the O1' atom of ADR11 (gray, 2) and (D) distance between the NZ atom of Lys(13) and the O1' atom of ADR2.

terminal base pairs were most frequently disoriented. One often observed, the “melted” configuration of the duplex head, is presented in Figure 8D, where APN1:dT12 bases are stacked and pulled out from the helix. The α -NH₃⁺ group is most often in interactions with the terminal base pairs (Figures 7C,D and 8C; see also Figures 2.5-, 2.8-, and 2.9 suppl of the Supporting Information).

Different helix head orientations were observed with *N*-methylmorpholinium-substituted PNA-2C and PNA-3C. In the PNA-2C-CO₁₂ duplex, the sterically hindered Lys(0)-MeMor head block does not reorient freely and the average conformation resembles that of the starting configuration, where the ϵ -NH₃⁺ group of Lys(0) points to the 3'-terminal OH group of DNA while the MeMor ring is exposed to the bulk aqueous phase without contacts with the PNA:DNA residues (Figure 2.6 suppl of the Supporting Information). In contrast, in the PNA-3C-CO₁₂ duplex, the sole MeMor ring initially reorients and interacts strongly (face-on) with the 2'-deoxyribose (dT12), so that the APN1 residue remains unpaired. Subsequently, it protrudes down along the minor groove, and thus, the whole duplex head is perturbed (Figure 2.7 suppl of the Supporting Information). Full chain stereoviews of various PNA:DNA duplex structures and other details are available as Supporting Information (Figures 2.4–2.9 suppl of the Supporting Information). The dynamic simulations of (Lys, NH₃⁺)PNA heteroduplexes with one or two nucleotide overhangs at the DNA ends showed stabilization of edge base pairing by providing less dynamically restricted electronegative

partner groups for the interaction with positively charged PNA caps, otherwise resulting in “fraying” of APN1:dT12 and TPN12:dT1 pairs (Figure 2.9 suppl of the Supporting Information). Importantly, in all MD-derived structures, the heteroduplex stem helix, encompassing all pairs, excluding the two head (APN1:dT12 and TPN2:dA11) and two tail (dT1:APN12 and dA2:TPN11) pairs, was unperturbed and always showed a robust Watson–Crick H-bonding pattern. Thus, the rmsd calculated for various averaged PNA:DNA 8-mer structures, i.e., via omission of the two head and two tail pairs, with the 1PDT 8-mer structure as a reference, gives a mass-weighted displacement of ≤ 1.6 Å. Interestingly, MD simulations of heteroduplexes composed of PNAs with uncharged caps, e.g., containing N-terminal acetyl and C-terminal amide groups only, presented structures of more robust Watson–Crick H-bonded base pairs at both termini.

DISCUSSION

In this work, we described previously unknown properties of Lys-, NH₂-, and MeMor-capped PNAs undergoing irreversible interstrand cross-linking reactions with DNA following γ -irradiation. The quantitative gel analysis shows that the overall ICL yield for a given PNA:DNA heteroduplex, depending on the applied radiation conditions, can be as high as 3–4% of the total DNA (*G* value $\sim 1 \times 10^3$ mol J⁻¹).

The data indicate that the mechanism of ICL formation involves formation of Schiff bases between PNA-based amino

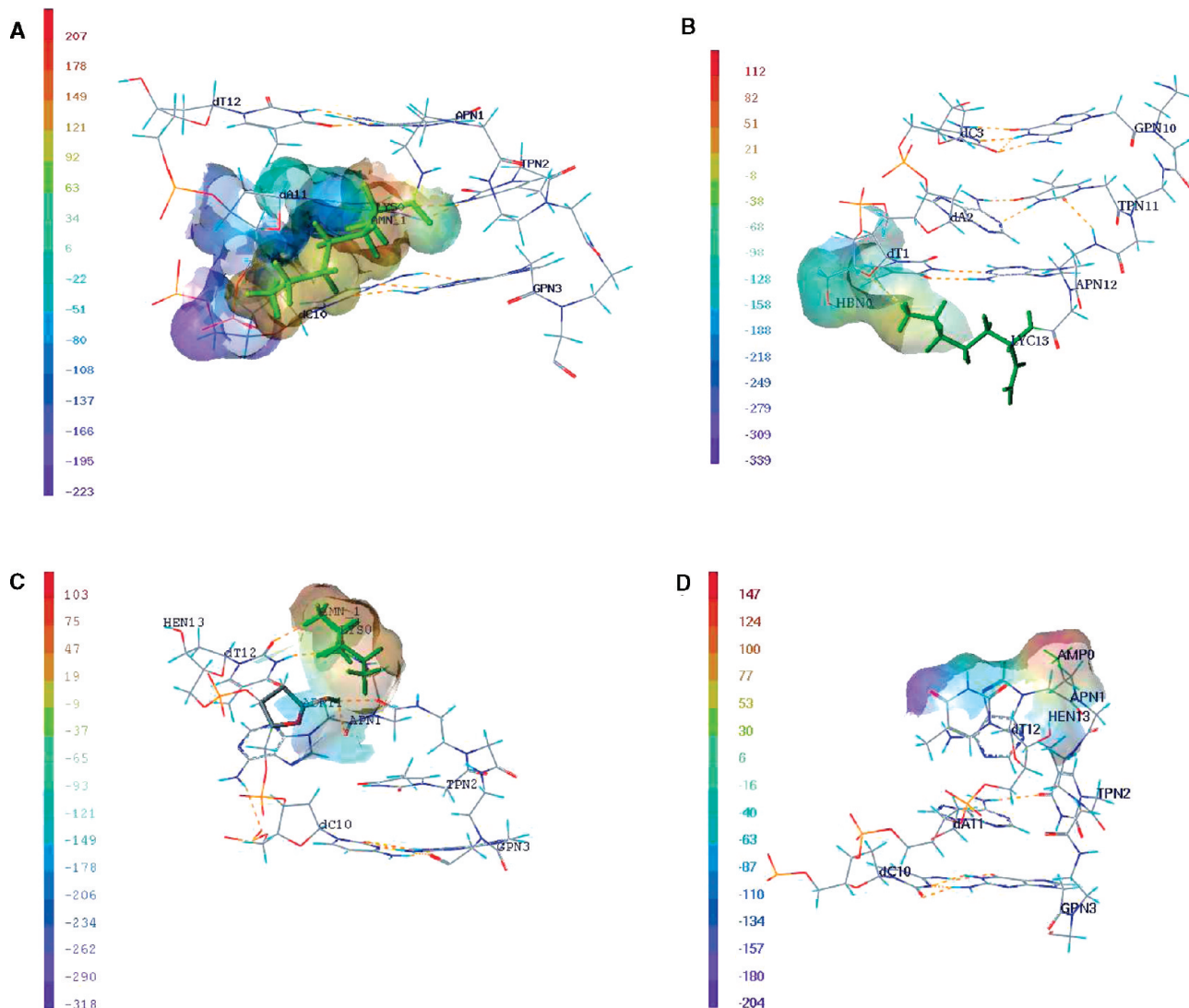
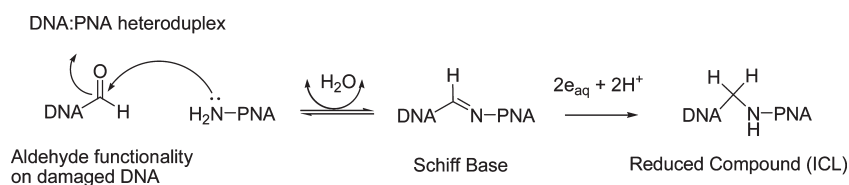


FIGURE 8: Orientation of the terminal residues and capping groups in different PNA:DNA duplexes (averaged structures of the last 50 ps of the 200 ps MD runs). PNA-1:CO₁₂ duplex: (A) the head blocking groups α -NH₃⁺ and ϵ -NH₃⁺ of Lys(0) are close to dC10 (2–4 Å), and (B) the NZ atom of Lys(13) is close (\sim 3.0 Å) to the O4' atom of dT1 (see also Figure 7). PNA-1:(AB2AB11)CO₁₂ duplex: (C) the nitrogen (NZ) atom of the head blocking group ϵ -NH₃⁺ of Lys(0) is \sim 3 Å distance from the O1' atom of ADR11, and the NH₃⁺ group is H-bonded to dT12 while the ADR11 O1' atom is H-bonded with APN1. (D) Single α -NH₃⁺ head configuration (AMP) of the PNA-3A:CO₁₂ duplex: the electrostatic interactions displace the APN1:dT12 base pair, and instead of being H-bonded, it is stacked. In all presented cases, the first and second base pairs are strongly perturbed, but the third pair from the either end and the duplex stem, in general, is not. Color-coded Connolly surfaces present the electric potential distribution in the regions of interest and show that the interactions are mostly electrostatic. As indicated by the color ramps (left, kilocalories per mole per electron) in different molecular configurations (encompassing also counterions and solvent), the electric potential varies. Capping groups (green) and ABS are in bold; H-bonds are represented as dashed orange lines.

Scheme 2



functional groups and radiation-damaged sites on DNA (ABS or modified bases). This type of covalent bonding is known and is widely accepted to take place in the formation of covalent links between NH₂ peptide (protein) groups and damaged (aldehydic) DNA sites, albeit in the presence of an exogenous reducing agent, such as NaBH₄ (26, 27). The new finding from this study is that apart from the prerequisite DNA damage, γ -radiation also provides reducing equivalents for transforming the initially

formed Schiff base linkage (imine) into a more stable reduced linkage (amine), i.e., to produce irreversible ICL (Scheme 2). This follows from the required abundance of solvated electrons, e_{aq}^- [the radiation-induced species with the highest reducing potential, $E_{\text{red}}^\circ = -2.9$ V (43)]. However, it is unclear if e_{aq}^- reduces the Schiff base directly or reduced base radicals, especially pyrimidine anions (low-reactive and long-lived in the absence of O₂), mediate the process. The latter possibility is

consistent with the results obtained with the MCO series (with overhangs) and CO₁₅, all emphasizing the importance of the 3'- and 5'-DNA terminal dT. Apart from the high reducing potential of thymine (44), this nucleobase has two other relevant properties. (i) Addition of $\cdot\text{OH}$ to the C5 position gives a C6-yl radical with reducing character (34), and (ii) various end products initiated by the attack of $\cdot\text{OH}$ on dT (5-formyl dU, ring-opened glycol, and hydantoin isomers) provide a large variety of aldehydic groups that may be involved in Schiff base formation. It is noteworthy that $\cdot\text{OH}$ radical-initiated damage to pyrimidine nucleotides accounts for $\sim 41\%$ of the strand breakage and 51% of the base release (formation of ABS), while e_{aq}^- is inefficient at producing strand breaks and can produce only minor damage to bases, resulting in $\sim 3\%$ of the base release induced by ionizing radiation (44). Under our typical experimental conditions (high dose of 750 Gy) and in the presence of $\cdot\text{OH}$ scavengers, we still obtain substantial DNA damage from $\cdot\text{OH}$ radicals revealed by the SSB ladder in the bottom part of sequencing gels (Figure 1A). Thus, although diminished, $\cdot\text{OH}$ -induced damage is incompletely scavenged. It follows that some $\cdot\text{OH}$ -mediated damage to DNA contributes to (e.g., to produce higher ABS yield) but is not sufficient for the formation of ICL; i.e., the presence of e_{aq}^- as a concomitant reducing radical is required for the generation of ICL. The findings in this study present a typical case of MDS production, where the synergism of the interactions of $\cdot\text{OH}$, e_{aq}^- , and possibly even $\cdot\text{H}$ radicals on the PNA:DNA heteroduplex results in ICL. Although e_{aq}^- is considered a relatively "harmless species" with respect to DNA damage, it is clearly less so in the case of PNA:DNA duplexes due to the significantly altered electrostatic potential surface of the latter. The charged PNA capping groups (Figures 6A and 8) with their extended positive electric field would drive the long-lived e_{aq}^- to the duplex end nucleotides, thus providing conditions for its preferential localization and reaction (41).

Our analysis was focused on the most intense interstrand cross-link production [ICL, I, II, III, and IV (Figure 1B)]. However, several diffuse bands with similar mobility also appear on the sequencing gels. It is possible that some of these bands arise from direct nucleotide–nucleotide cross-links, generated by a different mechanism (3). The ICL production with the participation of the ϵ - and α -amino groups of PNA lysinyl residues (ICL I–III) was anticipated; however, the appearance of band IV in PNA-3C:DNA duplexes only was surprising. It is not clear at this time how the methylmorpholinium engages in reactions of ICL with the DNA strand. On the other hand, ICL IV was not observed in PNA-2C, bearing both Lys and MeMor headgroups. The MD simulations gave a possible explanation by showing that when both charged groups are simultaneously present they tend to orient outward with respect to the duplex head (Figure 2.6 suppl of the Supporting Information), while when only MeMor is present, as in PNA-3C, it may well protrude into the minor groove (Figure 2.7 suppl of the Supporting Information).

Molecular modeling and molecular dynamics simulations provide information that improves our understanding of the role of PNA:DNA head and tail configuration and interactions. Previous PNA:DNA modeling and MD studies have focused on the characterization of the hallmark stem duplex properties, such as overall geometry, deviations, and/or similarity with the A- and B-DNA forms (46–48), thus complementing the experimental (22) and theoretical approaches (46, 48) which describe and attempt to predict the structural stability of PNA:DNA heteroduplexes. It is generally assumed that the higher stability of

PNA:DNA duplexes, as compared to that of DNA:DNA duplexes, is due to more favorable entropy change, attributed to counterion release (49). As follows from our results with N- and C-end-modified PNAs, the dangling end stabilization terms are especially important (22). It has been shown that only D-Lys incorporation stabilizes the PNA:DNA duplex, whereas L-Lys does not (20, 21, 50). It was found also that handedness of PNA:PNA duplexes depends on Lys chirality, but experimental (51) and modeling (52) studies emphasize that handedness is governed by steric rather than any specific interactions (H-bonding or electrostatic). Here we have found that all electrostatic, H-bonding, and steric interactions are involved in the preferential orientation of the (L-Lys, NH₂)PNA:DNA capping groups. We also found that the pronounced reorientation of the charged PNA caps not only perturbs the terminal Watson–Crick pairing but also can disorder the penultimate base pairs (Figure 8 and Figures 2.4–2.8 suppl of the Supporting Information). There is good conformity between our experimental and modeling results. Thus, with respect to the observed increased susceptibility of end nucleotides to free radical attack, MD data confirm that configurations where terminal bases are largely displaced into the solvent are common. The information obtained from the MD simulations also improves our understanding of the reason why ICL II which arise from Schiff base interactions of the α -NH₂ group are, in general, the most intense. This follows from the observed more frequent intrahelical protonated α -NH₃⁺–nucleobase close interactions, as compared with the nucleobase–(ϵ -NH₃⁺)Lys interactions. On the other hand, as shown for the range of normal and abasic PNA:DNA duplexes (Figures 7 and 8), the ϵ -NH₃⁺ groups of Lys(13) and Lys(0), when embedded in the minor groove, are within reach of dA2 (or AB2) and dA11 (or AB11), respectively. Therefore, it is reasonable to assume that the Schiff base partners of the two capping lysines (ICL bands I and III) are apurinic sites at the 5' and 3' DNA ends.

In conclusion, this study presents novel information about specific γ -radiation damage of (L-Lys, NH₂, and MeMor) end-modified PNA:DNA heteroduplexes, the generation of relatively high-yield PNA–DNA interstrand cross-links (ICL) as a part of MDS. Although ICL are often listed as potential highly toxic DNA lesions, there was scarce information about their production under radiation until recently (3–5). This work may provide new tools for studying PNA–DNA interactions. More importantly, our results may find applications in the development of a new generation of targeted radiosensitizers based on PNAs.

SUPPORTING INFORMATION AVAILABLE

Hybridization control and denaturing gel scans (Figures 1.1–1.3 suppl), computed PNA backbone charges (Figure 2.1 suppl), MD thermodynamic trajectories (Figures 2.2- and 2.3 suppl), stereo presentations of various full chain PNA:DNA heteroduplex structures obtained by MD simulations (Figures 2.4–2.9 suppl), and an example of the evaluation of the statistical significance between the results shown in Figures 2 and 3 (Table 1 suppl). This material is available free of charge via the Internet at <http://pubs.acs.org>.

REFERENCES

- (1) Hempel, K., and Mildenberger, E. (1987) Determination of G-values for single and double strand break induction in plasmid DNA using

- agarose gel electrophoresis and a curve-fitting procedure. *Int. J. Radiat. Biol.* 52, 125–138.
- (2) Rajski, S. R., and Williams, R. M. (1998) DNA cross-linking agents as antitumor drugs. *Chem. Rev.* 98, 2723–2795.
- (3) Regulus, P., Duroux, B., Bayler, P.-A., Favier, A., Cadet, J., and Ravanat, J.-L. (2007) Oxidation of the sugar moiety of DNA by ionizing radiation or bleomycin could induce the formation of a cluster DNA lesions. *Proc. Natl. Acad. Sci. U.S.A.* 104, 14032–14037.
- (4) Cecchini, S., Girouard, S., Huels, M. A., Sanche, L., and Hunting, D. J. (2004) Single-strand-specific radiosensitization of DNA by bromodeoxyuridine. *Radiat. Res.* 162, 604–615.
- (5) Cecchini, S., Girouard, S., Huels, M. A., Sanche, L., and Hunting, D. J. (2005) Interstrand cross-links: A new type of γ -ray damage in bromodeoxyuridine substituted DNA. *Biochemistry* 44, 1932–1940.
- (6) Cecchini, S., Masson, C., La Madeleine, C., Huels, M. A., Sanche, L., Wagner, J. R., and Hunting, D. J. (2005) Interstrand cross-link induction by UV radiation in bromodeoxyuridine-substituted DNA: Dependence on DNA conformation. *Biochemistry* 44, 16957–16966.
- (7) Dextraze, M.-E., Wagner, J. R., and Hunting, D. J. (2007) 5-Bromodeoxyuridine radiosensitization: Conformation-dependent DNA damage. *Biochemistry* 46, 9089–9097.
- (8) Gantchev, T. G., Cecchini, S., and Hunting, D. J. (2005) Dynamic Conformational States of DNA Containing T-T or T-BrdU Mismatched Bases: Wobble H-Bond Pairing vs. Cross-Strand Inter-Atomic Contacts. *J. Mol. Model.* 11, 141–159.
- (9) Nielsen, P. E. (1995) DNA analogues with nonphosphodiester backbones. *Annu. Rev. Biophys. Biomol. Struct.* 24, 167–183.
- (10) Eriksson, M., and Nielsen, P. E. (1996) PNA-nucleic acid complexes. Structure, stability and dynamics. *Q. Rev. Biophys.* 29, 369–394.
- (11) Porcheddu, A., and Giacomelli, G. (2005) Peptide nucleic acids (PNAs), A chemical overview. *Curr. Med. Chem.* 12, 2561–2599.
- (12) Nielsen, P. E., Egholm, M., and Buchardt, O. (1994) Sequence-specific transcription arrest by peptide nucleic acid bound to the DNA template strand. *Gene* 149, 139–145.
- (13) Mollegaard, N. E., Buchardt, O., Egholm, M., and Nielsen, P. E. (1994) Peptide nucleic acid-DNA strand displacement loops as artificial transcription promoters. *Proc. Natl. Acad. Sci. U.S.A.* 91, 3892–3895.
- (14) Ray, A., and Norden, B. (2000) Peptide nucleic acid (PNA): Its medical and biotechnical applications and promise for the future. *FASEB J.* 14, 1041–1060.
- (15) Nielsen, P. E. (2001) Peptide nucleic acid: A versatile tool in genetic diagnostics and molecular biology. *Curr. Opin. Biotechnol.* 12, 16–20.
- (16) Gambari, R. (2004) Biological activity and delivery of peptide nucleic acids (PNA)-DNA chimeras for transcription factor decoy (TFD) pharmacotherapy. *Curr. Med. Chem.* 11, 1253–1263.
- (17) Good, L., and Nielsen, P. E. (1998) Inhibition of translation and bacterial growth by peptide nucleic acid targeted to ribosomal RNA. *Proc. Natl. Acad. Sci. U.S.A.* 95, 2073–2076.
- (18) Marin, V. L., Roy, S., and Armitage, B. A. (2004) Recent advances in the development of peptide nucleic acid as a gene-targeted drug. *Expert Opin. Biol. Ther.* 4, 337–348.
- (19) Hu, J., and Corey, D. R. (2007) Inhibiting Gene Expression with PNA-Peptide Conjugates that Target Chromosomal DNA. *Biochemistry* 46, 7581–7589.
- (20) Sforza, S., Haaima, G., Marchelli, R., and Nielsen, P. E. (1999) Chiral peptide nucleic acids (PNAs): Helix handedness and DNA recognition. *Eur. J. Org. Chem.*, 197–204.
- (21) Menchise, V., De Simone, G., Tedeschi, T., Corradini, R., Sforza, S., Marchelli, R., Capasso, D., Saviano, M., and Pedone, C. (2003) Insights into peptide nucleic acid (PNA) structural features: The crystal structure of a D-lysine-based chiral PNA:DNA duplex. *Proc. Natl. Acad. Sci. U.S.A.* 100, 12021–12026.
- (22) Sugimoto, N., Satoh, N., Yasuda, K., and Nakano, S.-I. (2001) Stabilization factors affecting duplex formation of peptide nucleic acid with DNA. *Biochemistry* 40, 8444–8451.
- (23) Kilk, K., and Langel, U. (2005) Cellular delivery of peptide nucleic acid by cell-penetrating peptides. *Methods Mol. Biol.* 298, 131–141.
- (24) Rathinavelan, T., and Yathindra, N. (2005) Molecular dynamics structures of peptide nucleic acid DNA hybrid in the wild-type and mutated alleles of Ki-ras proto-oncogene. Stereochemical rationale for the low affinity of PNA in the presence of an A...C mismatch. *FEBS J.* 272, 4055–4070.
- (25) Yamanaka, K., Hayashi, H., Kato, K., Hasegawa, A., and Okada, S. (1995) Involvement of preferential formation of apurinic/apyrimidinic sites in dimethylarsenic-induced DNA strand breaks and DNA-protein crosslinks in cultured alveolar epithelial cells. *Biochem. Biophys. Res. Commun.* 207, 244–249.
- (26) Marchand, C., Neamati, N., and Pommier, Y. (2001) In vitro human immunodeficiency virus type 1 integrase assays. *Methods Enzymol.* 340, 624–633.
- (27) Mazumder, A., Neamati, N., Pilon, A. A., Sunder, S., and Pommier, Y. (1996) Chemical trapping of ternary complexes of human immunodeficiency virus type 1 integrase, divalent metal, and DNA substrates containing an abasic site. *J. Biol. Chem.* 271, 27330–27338.
- (28) Sugiyama, T., Kittaka, A., Takayama, H., Tomioka, M., Ida, Y., and Kuroda, R. (2003) Aggregation of RecA-derived peptides on single-stranded oligonucleotides triggered by Schiff base-mediated crosslinking. *Bioorg. Med. Chem. Lett.* 13, 2847–2851.
- (29) Marchand, C., Krajewski, K., Lee, H.-F., Antony, S., Johnson, A. A., Amin, R., Roller, P. P., Kvaratskhelia, M., and Pommier, Y. (2006) Covalent binding of the natural antimicrobial peptide indolicidin to DNA abasic sites. *Nucleic Acids Res.* 34, 5157–5165.
- (30) Sugiyama, H., Fujiwara, T., Ura, A., Tashiro, T., Yamamoto, K., Kawanishi, S., and Saito, I. (1994) Chemistry of thermal degradation of abasic sites in DNA. Mechanistic investigation on thermal DNA strand cleavage of alkylated DNA. *Chem. Res. Toxicol.* 7, 673–683.
- (31) Goljer, I., Kumar, S., and Bolton, P. H. (1995) Refined solution structure of a DNA heteroduplex containing an aldehydic abasic site. *J. Biol. Chem.* 270, 22980–22987.
- (32) Chen, J., Dupradeau, F.-Y., Case, D. A., Turner, C. J., and Stubbe, J. (2007) Nuclear magnetic resonance structural studies and molecular modeling of duplex DNA containing normal and 4'-oxidized abasic sites. *Biochemistry* 46, 3096–3107.
- (33) Wilde, J. A., Bolton, P. H., Mazumder, A., Manoharan, M., and Gerit, J. A. (1989) Characterization of the equilibrating forms of the aldehydic abasic site in duplex DNA by oxygen-17 NMR. *J. Am. Chem. Soc.* 111, 1894–1896.
- (34) von Sonntag, C. (1987) The chemical basis of radiation biology, Taylor & Francis, London.
- (35) Tremblay, S., Gantchev, T., Tremblay, L., Lavigne, P., Cadet, J., and Wagner, J. R. (2007) Oxidation of 2'-deoxycytidine to four interconverting diastereomers of N(1)-carbamoyl-4,5-dihydroxy-2-oximidazolidine nucleosides. *J. Org. Chem.* 72, 3672–3678.
- (36) Dedon, P. C. (2008) The chemical toxicology of 2-deoxyribose oxidation in DNA. *Chem. Res. Toxicol.* 21, 206–219.
- (37) Hudson, R. H. E., Liu, Y., and Wojciechowski, F. (2007) Hydrophilic modifications in peptide nucleic acid: Synthesis and properties of PNA possessing 5-hydroxymethyluracil and 5-hydroxymethylcytosine. *Can. J. Chem.* 85, 302–312.
- (38) Wojciechowski, F., and Hudson, R. H. E. (2008) Fluorescence and hybridization properties of peptide nucleic acid containing a substituted phenylpyrrolocytosine designed to engage guanine with an additional H-bond. *J. Am. Chem. Soc.* 130, 12574–12575.
- (39) Shishkina, I. G., and Johnson, F. (2000) A new method for the postsynthetic generation of abasic sites in oligomeric DNA. *Chem. Res. Toxicol.* 13, 907–912.
- (40) Eriksson, M., and Nielsen, P. E. (1996) Solution structure of a peptide nucleic acid-DNA duplex. *Nat. Struct. Biol.* 3, 410–413.
- (41) Gantchev, T. G., and Hunting, D. J. (2008) Probing the interactions of the solvated electron with DNA by molecular dynamics simulations: BUDR substituted normal DNA. *J. Mol. Model.* 14, 451–464.
- (42) Buxton, G. V., Greenstock, C. L., Helman, W. P., and Ross, A. B. (1988) Critical review of rate constants for reactions of hydrated electrons, hydrogen atoms and hydroxyl radicals ($\text{OH}^\bullet/\text{O}^\bullet$) in aqueous solution. *J. Phys. Chem. Ref. Data* 17, 513–886.
- (43) Wardman, P. (1989) Reduction potentials of one-electron couples involving free radicals in aqueous solution. *J. Phys. Chem. Ref. Data* 18, 1637–1755.
- (44) von Sonntag, C., and Schuchmann, H.-P. (1986) The radiolysis of pyrimidines in aqueous solutions: An updating review. *Int. J. Radiat. Biol.* 49, 1–34.
- (45) Ghaffari, M. A., Ali, H., Rousseau, J., and van Lier, J. E. (1997) Synthesis and tissue distribution of substituted [^{125}I]iodophenylamine derivatives: Possible brain imaging agents. *Nucl. Med. Biol.* 24, 151–164.
- (46) Sen, S., and Nilsson, L. (1998) Molecular dynamics of duplex systems involving PNA: Structural and dynamical consequences of the nucleic acid backbone. *J. Am. Chem. Soc.* 120, 619–631.
- (47) Srinivasan, A. R., and Olson, W. K. (1998) Molecular models of nucleic acid triple helices. I. DNA and RNA backbone complexes. *J. Am. Chem. Soc.* 120, 484–491.

- (48) Soliva, R., Sherer, E., Luque, F. J., Laughton, C. A., and Orozco, M. (2000) Molecular dynamics simulations of PNA:DNA and PNA:RNA duplexes in aqueous solution. *J. Am. Chem. Soc.* **122**, 5997–6008.
- (49) Tomac, S., Sarkar, M., Ratilainen, T., Wittung, P., Nielsen, P. E., Norden, B., and Grslund, A. (1996) Ionic effects on the stability and conformation of peptide nucleic acid complexes. *J. Am. Chem. Soc.* **118**, 5544–5552.
- (50) Haaime, G., Lohse, A., Buchardt, O., and Nielsen, P. E. (1996) Peptide nucleic acids (PNAs) containing thymine monomers derived from chiral amino acids: Hybridization and solubility properties of D-lysine PNA. *Angew. Chem., Int. Ed.* **35**, 1939–1942.
- (51) Wittung, P., Eriksson, M., Lyng, R., Nielsen, P. E., and Norden, B. (1995) Induced chirality in PNA-PNA duplexes. *J. Am. Chem. Soc.* **117**, 10167–10173.
- (52) Rasmussen, H., Liljefors, T., Petersson, B., Nielsen, P. E., and Kastrup, J. S. (2004) The influence of a chiral amino acid on the helical handedness of PNA in solution and in crystals. *J. Biomol. Struct. Dyn.* **21**, 495–502.